

Article

# Experimental Study of Electromagnetic-Assisted Rare-Earth Doped Yttrium Iron Garnet (YIG) Nanofluids on Wettability and Interfacial Tension Alteration

Zhen Yin Lau, Kean Chuan Lee <sup>\*</sup>, Hassan Soleimani and Hoe Guan Beh

Fundamental and Applied Sciences Department, Universiti Teknologi PETRONAS, 32610 Seri Iskandar, Perak, Malaysia; lau.zhen\_23150@utp.edu.my (Z.Y.L.); hassan.soleimani@utp.edu.my (H.S.); beh.hoeguan@utp.edu.my (H.G.B.)

\* Correspondence: lee.kc@utp.edu.my

Received: 29 August 2019; Accepted: 27 September 2019; Published: 9 October 2019



**Abstract:** Applications of nanoparticles (NPs) in the Enhanced oil recovery (EOR) method has become a major research field as nanoparticles are found to be able to interfere with the interfacial tension and wettability of multiphase fluids within the reservoir formation with or without the irradiance of the electromagnetic (EM) waves. For future EOR usage, a material with high temperature stability and low losses under oscillating wave is recommended, Yttrium Iron Garnet (YIG). This paper describes the synthesis of rare-earth doped YIG (RE-YIG, RE = (Lanthanum (La), Neodymium (Nd) and Samarium (Sm))) and the roles of rare-earth in alteration of magnetic properties. These magnetic properties are believed to have direct relation with the change in wettability, viscosity and interfacial tension of YIG nanofluids. Here we prepared the  $Y_{2.8}R_{0.2}Fe_5O_{12}$  (R = La, Nd, Sm) NPs using the sol-gel auto-combustion technique and further annealed at 1000 °C for 3 h. The Field Emission Scanning Electron Microscope (FESEM) images reveal the particles having grain size ranging from 100–200 nm with high crystallinity and X-ray Powder Diffraction (XRD) shows varying shift of the peak position due to the bigger size of the rare-earth ions which resulted in structural distortion. The wettability of the nanofluid for all samples shows overall reduction under the influence of EM waves. On the other hand, the interfacial tension (IFT) and viscosity of RE-YIG nanofluids has lower value than the pure YIG nanofluids and decreases when the ionic radius of rare-earth decreases. Sm-YIG has the highest magnitude in IFT and magnetization saturation of 23.54 emu/g which suggests the increase in magnetization might contribute to higher surface tension of oil-nanofluid interface.

**Keywords:** nanofluid; wettability; IFT; magnetic; rare-earths

## 1. Introduction

Enhanced oil recovery (EOR) using the nanoparticles method has been a major novel application research topic to further improve current oil recovery rate. According to Bennetzen [1] and Peng [2], nanoparticles have shown promising solution to both upstream and downstream of oil and gas field, among which are the ability to alter wettability, interfacial tension (IFT) and viscosity of the multiphase fluids within the reservoir formation. Injection of nanoparticles as nanofluids into reservoir formation under the influence of electromagnetic (EM) wave will activate the nanoparticles to cause thermodynamics disturbance within the reservoir structure [3]. Low dimensionality of nanoparticles enhanced the magnetization or became paramagnetic, which makes alteration of surface force of fluids achievable [4] and improves the recovery rate through oil-water IFT reduction [5]. To further improve oil recovery rate, the magnetic aspect of nanoparticles is crucial. Oscillating magnetization forces

experienced by the magnetic nanoparticles has been shown to initiate interfacial movement at the oil-water interface, and altering the apparent viscosity of the nanofluids due to their magnetorheological and electrorheological properties, which improve the oil mobilization rate [6–9]. In a simulation study [10], high magnetic susceptibility nanoparticles were recommended as the magnetic perturbation caused by nanoparticles within the pore wall will facilitate oil blob detachment, thus improving the oil recovery rate. As in Soleimani et al. [11], higher magnetic susceptibility nanoparticles show better oil recovery rate in a core flooding test under EM wave irradiance.

A core flooding test with Yttrium Iron Garnet (YIG) nanofluid with the presence of EM waves has shown a yield of 43.64% [12], making them a promising candidate for the application. Rare-earths (RE) doped YIG has shown promising ability to alter the magnetic properties of YIG, changing the structural, morphological and dielectric properties as well [13]. However, the dopant alteration of the magnetic properties of YIG is dependent on the magnetic moment of both rare-earth ions and yttrium ions, observed neodymium doped YIG has a higher magnetic properties than YIG [14]. Low dimensionality of YIG nanoparticles shows superparamagnetic behavior with high magnetic susceptibility as well [15].

Hence, in this study, rare-earths Lanthanum (La), Neodymium (Nd) and Samarium (Sm) were doped into YIG at the concentration of 0.2 mol, to form  $Y_{2.8}R_{0.2}Fe_5O_{12}$  (RE-YIG) nanoparticles and the samples are defined as La-YIG, Nd-YIG and Sm-YIG, respectively. The samples were synthesized via sol-gel auto-combustion method and characterized with Field Emission Scanning Electron Microscope (FESEM), Energy-Dispersive X-ray (EDX), X-ray Powder Diffraction (XRD) and Vibrating-Sample Magnetometer (VSM). The RE-YIG nanofluids properties were evaluated through inverted sessile drop method for contact angle and IFT data. Viscosity of the RE-YIG nanofluids were done using a rheometer. The investigation of RE-YIG nanofluids properties has not been reported elsewhere. All nanofluids evaluation were done with or without the EM irradiance of 100 MHz.

## 2. Methodology

### 2.1. Materials and Methods

Yttrium (III) Nitrate, Lanthanum (III) Nitrate, Neodymium (III) Nitrate, Samarium (III) Nitrate and Iron (III) Nitrate were used as raw materials to synthesize the RE-YIG nanoparticles via sol-gel auto-combustion method. Citric acid was added as chelating agent at the ratio of metal nitrates to citrates to be 1:1 [16], and the pH of the mixture solution was adjusted to 2 using ammonia solution [17]. The resulting solutions were then heated at 90 °C and stirred with magnetic stirrer until a viscous gel is formed. The gel was then heated up to 250–300 °C until auto-combustion occurs and the burnt powder was then grounded. The powder was further annealed at 1000 °C for 3 h. For complete annealing treatment and the formation of single phase high crystallinity YIG nanoparticles, high annealing temperature is required [18–20].

### 2.2. Characterization of RE-YIG Nanoparticles

Once RE-YIG NPs were synthesized, FESEM coupled EDX were performed to characterize their morphology and element composition. XRD spectroscopy was also carried out to evaluate the phase and crystallinity of the synthesized RE-YIG NPs. As for the magnetization properties of the samples, they were characterized using VSM.

### 2.3. Evaluation of RE-YIG Nanofluids

In order to form nanofluid samples, 0.01 wt% of RE-YIG nanoparticles were mixed with 30,000 ppm brine solution [21]. Then, 0.05 wt% of surfactant (sodium dodecylbenzenesulfonate/SDBS) was added to increase the suspension time of the NPs within the fluid. Once the nanofluids were prepared, their densities were measured using density bottle. For the evaluation of wettability and IFT, an inverted sessile drop method was used with the help of Goniometer [22] to measure the oil-wetting contact angle and IFT of the oil-nanofluids interface, both with and without the presence of EM waves.

The oil is dropped on glass surface treated with propanol and UV immersed in nanofluid. The light crude-oil with density of 0.925 g/mL is used (Tapis field, Malaysia). Viscosity of nanofluids was also measured using rheometer with and without EM waves.

### 3. Results and Discussions

#### 3.1. Characterization of RE-YIG Nanoparticles

FESEM & EDX: As shown in Figure 1a–d, the measure grain size of NPs synthesized were within the range of 100–200 nm. Along with the FESEM results, EDX data were collected and tabulated in Table 1. EDX results show the element composition of each sample matches well with the weight percent of rare-earths doped in YIG which is about 3% corresponding to the 0.2 mole concentration.

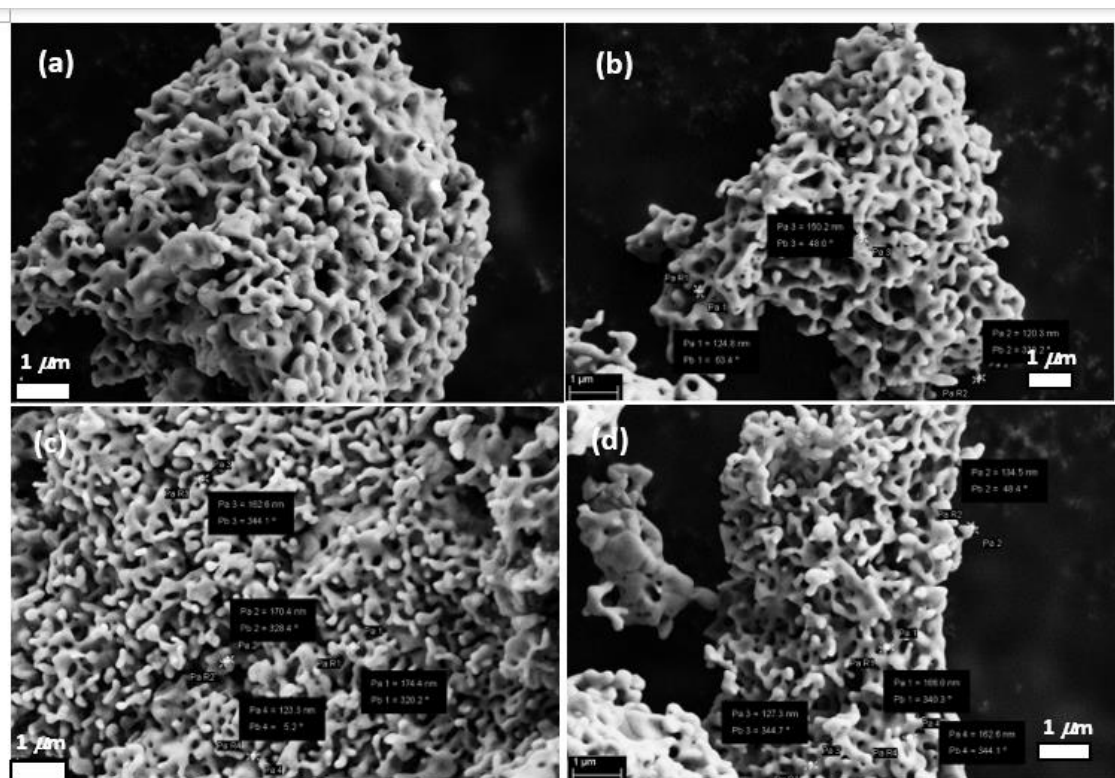


**Figure 1.** Field mission Scanning Electron Microscope (FESEM) images for (a) YIG, (b) La-YIG, (c) Nd-YIG and (d) Sm-YIG.

**Table 1.** Weight percentage analysis of  $Y_{2.8}R_{0.2}Fe_5O_{12}$  (RE-YIG) samples.

Element	Samples (Weight %)			
	YIG	La-YIG	Nd-YIG	Sm-YIG
Y	34.37	31.44	33.19	33.38
Fe	29.89	30.95	26.05	30.18
O	35.73	34.11	38.15	32.64
RE	0	3.49	2.61	3.8

XRD: Referring to ICDD PDF2 RDB database, it was found that YIG with chemical formula of  $Y_3Fe_5O_{12}$  with a cubic crystal system were formed along with small traces of YIG with chemical formula of  $YFeO_3$  which is orthorhombic crystal system. Figure 2 shows the XRD patterns of YIG and RE-YIG NPs respectively, where hkl values were obtained. from the database. High intensity peaks shown in Figure 2 indicate high crystallinity properties of the NPs.

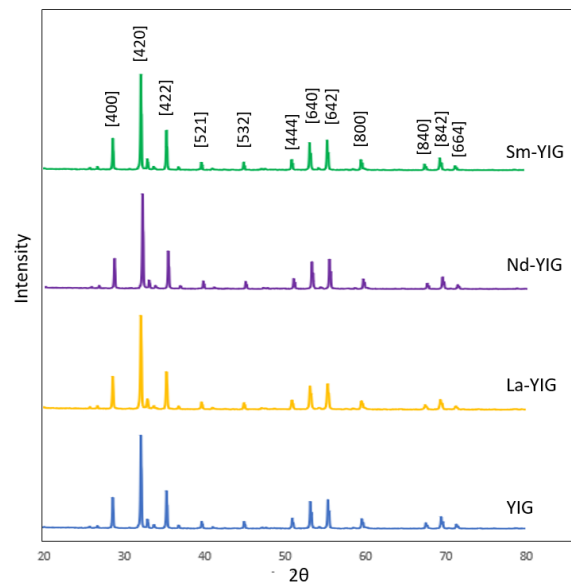


**Figure 2.** X-ray Powder Diffraction (XRD) pattern of RE-YIG nanoparticles.

Based on the highest peak (420) of the spectrum, the  $2\theta$ , Full-width Half-maximum (FWHM) and  $d$ -spacing values crystalline size was calculated using Scherrer equation

$$D = \frac{k\lambda}{\beta \cos \theta} \quad (1)$$

where  $D$  represents the crystalline size,  $k$  is the shape factor (0.89),  $\lambda$  is the laser source wavelength (1.5406 Å for Cu K $\alpha$ ),  $\beta$  is the FWHM value of the peak and  $\theta$  is the Bragg's angle.

$$d_{hkl} = \frac{a}{\sqrt{h^2 + k^2 + l^2}} \quad (2)$$

Equation (2) was then used to calculate the lattice parameter of the synthesized samples, where  $d_{hkl}$  is the distance between the planes of atoms that give rise to the diffraction peaks,  $a$  is the lattice parameter of the crystal lattice and  $h$ ,  $k$  and  $l$  are the Miller indices of the plane.

Both the measured and calculated values were tabulated in Table 2. It was observed that the crystalline size of the RE-YIG NPs was within the range of 45–53 nm. Besides that, we also found there has been a variation in  $2\theta$  and lattice constant value with different rare-earths dopants. It is speculated that the different ionic size of the rare-earth metals and yttrium contributes to such variation [13]. Lattice constant increased in the sequence of YIG, Sm-YIG, Nd-YIG and La-YIG, corresponding to the increase in ionic size of the metal ions.

**Table 2.** Measured and calculated parameter of RE-YIG nanoparticles based on (420) peak.

Samples	$2\theta$	FWHM (°)	Crystalline Size, D (nm)	D-Spacing (Å)	Lattice Constant, $a$
YIG	32.324	0.163	50.058	2.767	12.374
La-YIG	32.272	0.182	44.879	2.771	12.393
Nd-YIG	32.298	0.158	51.870	2.769	12.383
Sm-YIG	32.324	0.154	53.062	2.768	12.377

VSM: Magnetic properties were studied by using VSM measurements performed at room temperature. As observed in Figure 3, RE-YIG shows soft magnetic material features whereby they can be magnetized and demagnetized easily with almost no loss, indicating the existence of superparamagnetic and single domain particles in the samples [23–25].

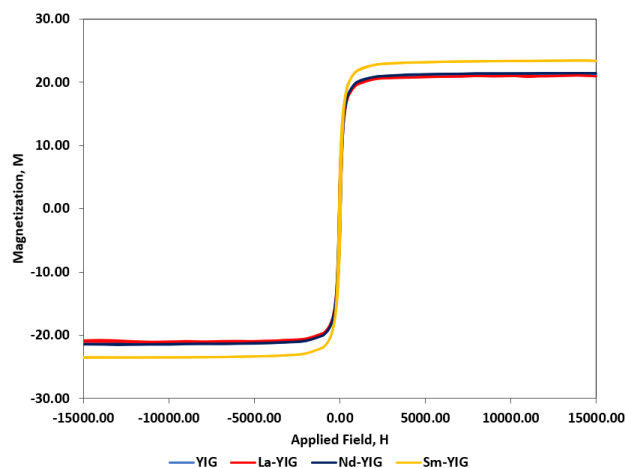


Figure 3. Magnetic hysteresis loop of RE-YIG nanoparticles.

Furthermore, as tabulated in Table 3 and Figure 4, the magnetic saturation ( $M_r$ ) of YIG decreases with the doping of La and increases with the doping of Nd and Sm, indicating that Nd and Sm have the parallel magnetic moment alignment with Y ion in YIG structure, as in Wolf and Uhm et al. [14,26]. Magnetic remanence ( $M_r$ ), coercivity ( $H_c$ ) and saturation ( $H_s$ ) has shown a general increases from YIG, La-YIG, Nd-YIG and Sm-YIG, following the order as per mentioned. The coercivity was observed to be increased as well. However, RE-YIG NPs are still considered as soft magnetic materials with  $H_c$  less than 100 Oe.

Table 3. Properties of RE-YIG nanoparticles.

Samples	Magnetic Parameters			
	$M_s$ (emu/g)	$M_r$ (emu/g)	$H_c$ (Oe)	$H_s$ (Oe)
YIG	21.30	4.45	37.09	1395.97
La-YIG	21.10	4.41	39.68	1429.42
Nd-YIG	21.50	5.25	46.05	1464.67
Sm-YIG	23.54	6.02	47.03	1503.88

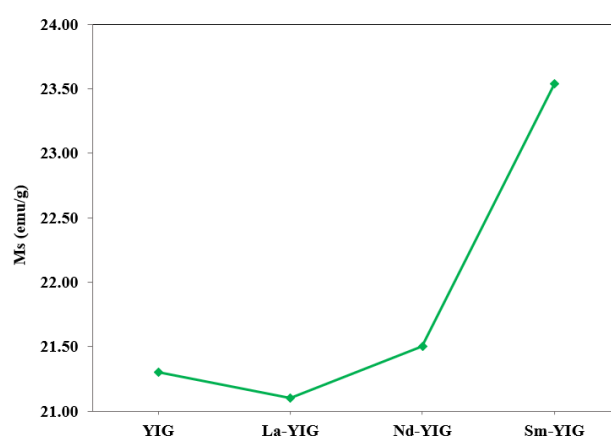
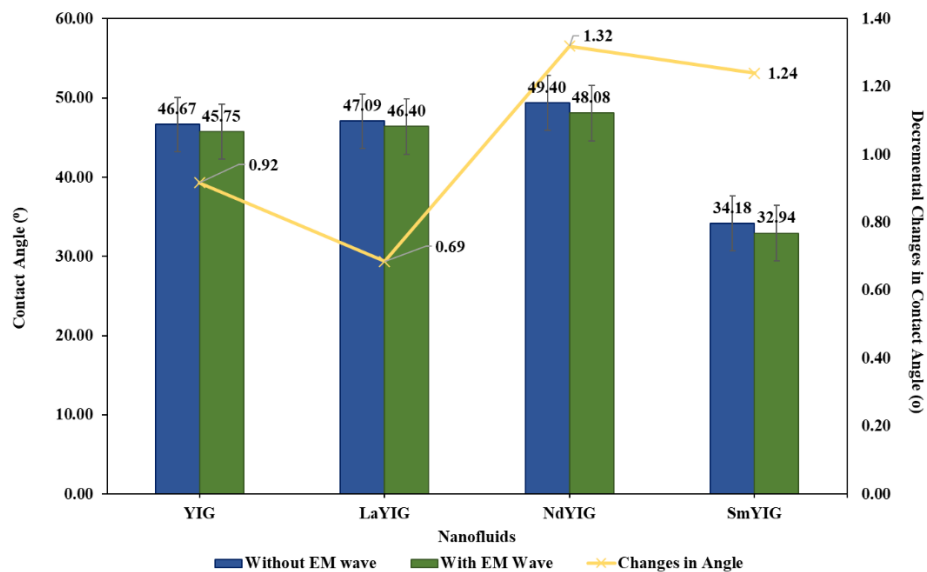


Figure 4. Variation of magnetic saturation with RE-YIG samples.

### 3.2. Evaluation of RE-YIG Nanofluids.

Wettability: Oil-wetting alteration were measured using inverted sessile drop contact angle measurement method with Goniometer. Figure 5 shows that La-YIG and Nd-YIG nanofluids have a slightly higher initial contact angle than YIG nanofluid, whereas Sm-YIG nanofluid shows significant reduction, even without the irradiance of Electromagnetic (EM) waves. We suspect that

the electrorheological properties of Sm-YIG nanofluids has contributed to the significant difference. Overall, RE-YIG has shown a general reduction in oil-wetting angle, indicating a better performance of oil sweeping rate [27–30].



**Figure 5.** Contact angle for RE-YIG samples with and without EM waves.

IFT: Based on Figure 6, it is observed that the oil-nanofluid IFT results does not show significant changes under the influence, of EM wave. However, the IFT value does differ for different rare-earth dopants. La-YIG has the lowest IFT value whereas Sm-YIG has the highest one. The increase in IFT value is attributed to the increase in rare-earth metal ionic size, suggesting that the structural properties of RE-YIG are contributors to the IFT alteration, which requires further study.

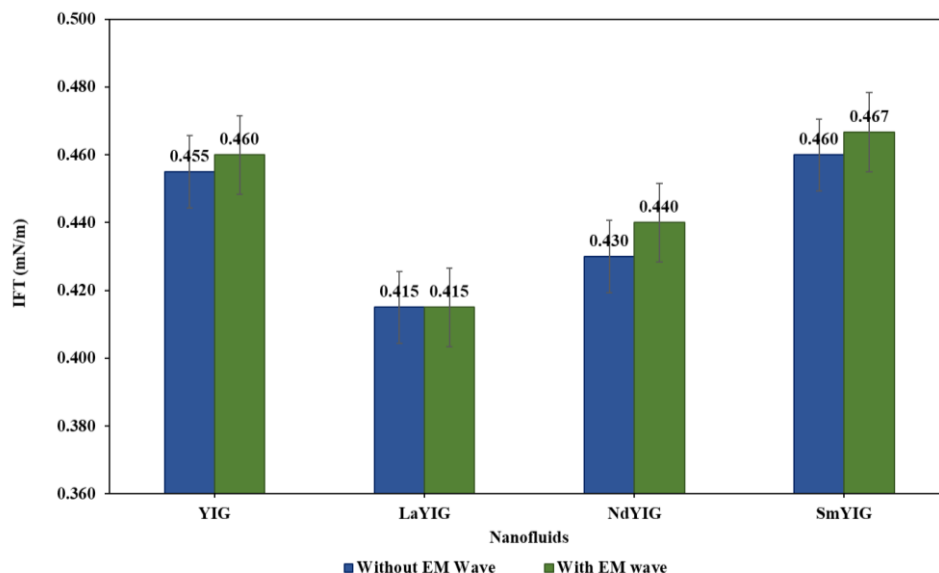


**Figure 6.** Interfacial tension (IFT) for RE-YIG samples with and without EM waves.

Viscosity: As shown in Figure 7, a similar trend of viscosity of RE-YIG without the influence of EM wave were observed as in IFT section, further suggesting that the structural properties of RE-YIG should be investigated. Under the irradiance of EM waves, each RE-YIG nanofluid shows different magnitude in changes of viscosity as well, with La-YIG having the largest increment, which is 3.61% followed by Nd-YIG. It is suspected that the structural distortion experienced by the YIG structure due

to the doping of bigger ionic size metal ions and the magnetic coercivity of RE-YIG particle are the main factors contributing to the variation of incremental change in viscosity.

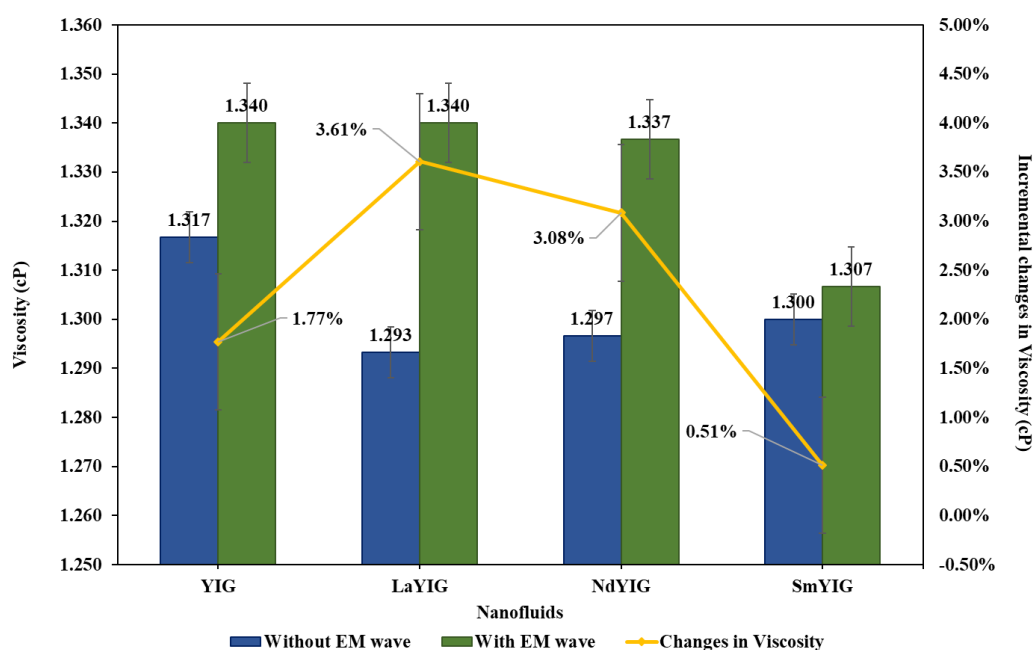


Figure 7. Viscosity for RE-YIG samples with and without EM waves.

#### 4. Conclusion

A high crystallinity  $Y_{2.8}Re_{0.2}Fe_5O_{12}$  (RE = La, Nd, Sm) with grain size ranging between 100–200 nm were synthesized successfully via the sol-gel auto-combustion method. XRD results showed variation in lattice parameter, suggesting the ionic radii of rare-earth metal ions contributed to structural distortion within the YIG structure which increased the overall lattice constant of the crystal structure. Nd-YIG and Sm-YIG shown improvement in YIG magnetization saturation value, with Sm-YIG being 23.54 emu/g. Wettability data showed general improvement in reduction of oil-wetting contact angle, suggesting potential improvement in oil sweeping rate. Both IFT and viscosity data showed that the dopant of the YIG nanoparticles contributes to the changes in IFT and viscosity value without the irradiance of EM waves. Under the influence of EM waves, IFT value does not alter significantly. La-YIG showed the highest increment in viscosity value at 3.61% followed by Nd-YIG, YIG and Sm-YIG. Both structural and magnetic properties of RE-YIG are suspected to contribute to such changes, where further research studies are recommended.

In conclusion, the doping of rare-earth metal ions into YIG structure will change the various parameters and properties of the YIG nanoparticles and hence alter the IFT, wettability and viscosity when applied as nanofluids in EOR applications.

**Author Contributions:** Conceptualization, K.L.; Methodology, Z.L.; Validation, K.L., H.S. and H.B.; Formal Analysis, K.L.; Writing—Original Draft Preparation, Z.L.; Writing—Review & Editing, K.L.; Supervision, K.L., H.S. and H.B.; Project Administration, K.L.

**Funding:** The authors would like to acknowledge Yayasan Universiti Teknologi PETRONAS (YUTP) (015LC0-143) for funding the research.

**Conflicts of Interest:** The authors declare no conflict of interest.

#### References

1. Bennetzen, M.V.; Mogensen, K. Novel Applications of Nanoparticles for Future Enhanced Oil Recovery. In Proceedings of the International Petroleum Technology Conference, Kuala Lumpur, Malaysia, 10–12 December 2014.

2. Peng, B.; Tang, J.; Luo, J.; Wang, P.; Ding, B.; Tam, K.C. Applications of Nanotechnology in Oil and Gas Industry: Progress and Perspective. *Can. J. Chem. Eng.* **2018**, *96*, 91–100. [[CrossRef](#)]
3. Bhatia, K.H.; Chacko, L.P. Ni-Fe Nanoparticles: A Innovative Approach for Recovery of Hydrates. In *Brasil Offshore*; Society of Petroleum Engineers: Richardson, TX, USA, 2011.
4. Pilkington, G.A.; Briscoe, W.H. Nanofluids mediating surface forces. *Adv. Colloid Interface Sci.* **2012**, *179*, 68–84. [[CrossRef](#)]
5. Soleimani, H.; Baig, M.K.; Yahya, N.; Khodapanah, L.; Sabet, M.; Demiral, B.M.; Burda, M. Synthesis of ZnO nanoparticles for oil-water interfacial tension reduction in enhanced oil recovery. *Appl. Phys. A* **2018**, *124*, 128. [[CrossRef](#)]
6. Ryoo, S.; Rahmani, A.R.; Yoon, K.Y.; Prodanović, M.; Kotsmar, C.; Milner, T.E.; Huh, C.; Johnston, K.P.; Bryant, S.L. Theoretical and experimental investigation of the motion of multiphase fluids containing paramagnetic nanoparticles in porous media. *J. Pet. Sci. Eng.* **2012**, *81*, 129–144. [[CrossRef](#)]
7. Yahya, N.; Kashif, M.; Shafie, A.; Soleimani, H.; Zaid, H.M.; Latiff, N.R.A. Improved Oil Recovery by High Magnetic Flux Density Subjected to Iron Oxide Nanofluids. *J. Nano Res.* **2014**, *26*, 89–99. [[CrossRef](#)]
8. Zitha, P.; Wessel, F. *Fluid Flow Control Using Magnetorheological Fluids*; Society of Petroleum Engineers Inc.: Richardson, TX, USA, 2002.
9. Zaid, H.M.; Latiff, N.R.A.; Yahya, N.; Soleimani, H.; Shafie, A. Application of electromagnetic waves and dielectric nanoparticles in enhanced oil recovery. *J. Nano Res.* **2014**, *26*, 135–142. [[CrossRef](#)]
10. Soares, F.S.M.D.A.; Prodanovic, M.; Huh, C. Excitable Nanoparticles for Trapped Oil Mobilization. In *SPE Improved Oil Recovery Symposium*; Society of Petroleum Engineers: Richardson, TX, USA, 2014.
11. Soleimani, H.; Yahya, N.; Latiff, N.R.A.; Zaid, H.M.; Demiral, B.; Amighian, J. Novel Enhanced Oil Recovery Method using  $\text{Co}_2 + x\text{Fe}_2 + (1-x)\text{Fe}_3 + 2\text{O}_4$  as Magnetic Nanoparticles Activated by Electromagnetic Waves. *J. Nano Res.* **2014**, *26*, 111–116. [[CrossRef](#)]
12. Soleimani, H.; Latiff, N.R.A.; Yahya, N.; Sabet, M.; Khodapanah, L.; Kozlowski, G.; Guan, B.H.; Chuan, L.K. Synthesis and Characterization of Yttrium Iron Garnet (YIG) Nanoparticles activated by Electromagnetic wave in Enhanced Oil Recovery. *J. Nano Res.* **2016**, *38*, 40–46. [[CrossRef](#)]
13. Akhtar, M.N.; Yousaf, M.; Khan, S.N.; Nazir, M.S.; Ahmad, M.; Khan, M.A. Structural and electromagnetic evaluations of YIG rare earth doped (Gd, Pr, Ho, Yb) nanoferrites for high frequency applications. *Ceram. Int.* **2017**, *43*, 17032–17040. [[CrossRef](#)]
14. Wolf, W. Ferromagnetic Alignment by Antiferromagnetic Exchange Interaction. Note on the Magnetic Behaviour of Neodymium Garnet. *J. Appl. Phys.* **1961**, *32*, 742. [[CrossRef](#)]
15. Sánchez, R.D.; Rivas, J.; Vaqueiro, P.; Lopez-Quintela, M.A.; Caeiro, D. Particle size effects on magnetic properties of yttrium iron garnets prepared by a sol-gel method. *J. Magn. Magn. Mater.* **2002**, *247*, 92–98. [[CrossRef](#)]
16. Vajargah, S.H.; Hosseini, H.M.; Nemati, Z.A. Preparation and characterization of yttrium iron garnet (YIG) nanocrystalline powders by auto-combustion of nitrate-citrate gel. *J. Alloys Compd.* **2007**, *430*, 339–343. [[CrossRef](#)]
17. Vajargah, S.H.; Hosseini, H.M.; Nemati, Z.A. Synthesis of nanocrystalline yttrium iron garnets by sol-gel combustion process: The influence of pH of precursor solution. *Mater. Sci. Eng. B* **2006**, *129*, 211–215. [[CrossRef](#)]
18. Vaqueiro, P.; Lopez-Quintela, M.A.; Rivas, J.; Greneche, J.M. Annealing dependence of magnetic properties in nanostructured particles of yttrium iron garnet prepared by citrate gel process. *J. Magn. Magn. Mater.* **1997**, *169*, 56–68. [[CrossRef](#)]
19. Akhtar, M.N.; Khan, M.A.; Ahmad, M.; Murtaza, G.; Raza, R.; Shaikat, S.F.; Raza, M.R.; Asif, M.H.; Nasir, N.; Abbas, G.; et al.  $\text{Y}_3\text{Fe}_5\text{O}_{12}$  nanoparticulate garnet ferrites: Comprehensive study on the synthesis and characterization fabricated by various routes. *J. Magn. Magn. Mater.* **2014**, *368*, 393–400. [[CrossRef](#)]
20. Janifer, M.A.; Anand, S.; Senthuran, M.; Pauline, S. Effect of synthesis conditions on yttrium iron garnet (YIG) nanocrystalline powder via sol-gel method. *Int. Res. J. Eng. Technol. (IRJET)* **2017**, *4*, 78–81.
21. Ogolo, N.A.; Olafuyi, O.A.; Onyekonwu, M.O. Enhanced Oil Recovery Using Nanoparticles. In *SPE Saudi Arabia Section Technical Symposium and Exhibition*; Society of Petroleum Engineers: Richardson, TX, USA, 2012.
22. Yuan, Y.; Lee, T.R. Chapter 1: Contact angle and wetting properties. In *Surface Science Techniques*; Springer: Berlin/Heidelberg, Germany, 2013; pp. 3–34.

23. Herzer, G. Grain size dependence of coercivity and permeability in nanocrystalline ferromagnets. *IEEE Trans. Magn.* **1990**, *26*, 1397–1402. [[CrossRef](#)]
24. Kneller, E.F.; Luborsky, F.E. Particles Size Dependence of Coercivity and Remanence of Single Domain Particles. *J. Appl. Phys.* **1963**, *34*, 656–658. [[CrossRef](#)]
25. Lu, A.H.; Salabas, E.E.; Schüth, F. Magnetic Nanoparticles: Synthesis, Protection, Functionalization, and Application. *Angew. Chem. Int. Ed.* **2007**, *46*, 1222–1244. [[CrossRef](#)]
26. Uhm, Y.R.; Lim, J.C.; Choi, S.M.; Kim, C.S. Magnetic Properties of R-YIG (R = La, Nd, and Gd) Derived by a Sol-gel Method. *J. Magn.* **2016**, *21*, 303–307. [[CrossRef](#)]
27. Mohajeri, M.; Hemmati, M.; Shekarabi, A.S. An experimental study on using a nanosurfactant in an EOR process of heavy oil in fractured micromodel. *J. Pet. Sci. Eng.* **2015**, *126*, 162–173. [[CrossRef](#)]
28. Mittal, N.; Deva, D.; Kumar, R.; Sharma, A. Exceptionally robust and conductive superhydrophobic free-standing films of mesoporous carbon nanocapsule/polymer composite for multifunctional applications. *Carbon* **2015**, *93*, 492–501. [[CrossRef](#)]
29. Mittal, N.; Kumar, R.; Mishra, G.; Deva, D.; Sharma, A. Mesoporous carbon nanocapsules based coatings with multifunctionalities. *Adv. Mater. Interfaces* **2016**, *3*, 1500708. [[CrossRef](#)]
30. Brett, C.J.; Mittal, N.; Ohm, W.; Gensch, M.; Kreuzer, L.P.; Körstgens, V.; Roth, S.V. Water Induced Structural Rearrangements on the Nanoscale in Ultrathin Nanocellulose Films. *Macromolecules* **2019**, *52*, 4721–4728. [[CrossRef](#)]



© 2019 by the authors. Licensee MDPI, Basel, Switzerland. This article is an open access article distributed under the terms and conditions of the Creative Commons Attribution (CC BY) license (<http://creativecommons.org/licenses/by/4.0/>).